

RESEARCH ARTICLE | FEBRUARY 05 2024

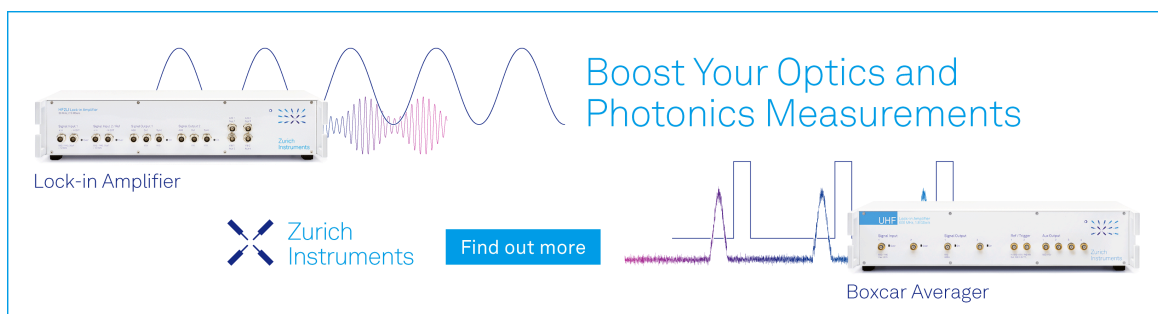
The ultraviolet and vacuum ultraviolet absorption spectrum of gamma-pyrone; the singlet states studied by configuration interaction and density functional calculations

Michael H. Palmer ; Søren Vrønning Hoffmann ; Nikola C. Jones ; Marcello Coreno ; Monica de Simone ; Cesare Grazioli ; R. Alan Aitken ; Loëlia Perrault ; Iain L. J. Patterson 




J. Chem. Phys. 160, 054305 (2024)

<https://doi.org/10.1063/5.0186919>



Boost Your Optics and Photonics Measurements

Lock-in Amplifier

 Zurich Instruments

[Find out more](#)

Boxcar Averager

The ultraviolet and vacuum ultraviolet absorption spectrum of gamma-pyrone; the singlet states studied by configuration interaction and density functional calculations

Cite as: J. Chem. Phys. 160, 054305 (2024); doi: 10.1063/5.0186919

Submitted: 9 November 2023 • Accepted: 5 January 2024 •

Published Online: 5 February 2024



View Online



Export Citation



CrossMark

Michael H. Palmer,^{1,a)} Søren Vrønning Hoffmann,^{2,b)} Nikola C. Jones,^{2,c)} Marcello Coreno,^{3,d)}
Monica de Simone,^{4,e)} Cesare Grazioli,^{4,f)} R. Alan Aitken,^{5,g)} Loëlia Perrault,^{5,h)}
and Iain L. J. Patterson^{5,i)}

AFFILIATIONS

¹School of Chemistry, University of Edinburgh, Joseph Black Building, David Brewster Road, Edinburgh, EH9 3FJ Scotland, United Kingdom

²ISA, Department of Physics and Astronomy, Aarhus University, Ny Munkegade 120, DK-8000 Aarhus C, Denmark

³ISM-CNR, Istituto di Struttura della Materia, LD2 Unit, 34149 Trieste, Italy

⁴IOM-CNR, Istituto Officina dei Materiali, Basovizza SS-14, Km 163.5, 34149 Trieste, Italy

⁵School of Chemistry, University of St Andrews, North Haugh, St Andrews, Fife, KY16 9ST Scotland, United Kingdom

^{a)} Author to whom correspondence should be addressed: m.h.palmer@ed.ac.uk

^{b)} Electronic mail: vrønning@phys.au.dk

^{c)} Electronic mail: nykj@phys.au.dk

^{d)} Electronic mail: marcello.coreno@elettra.eu

^{e)} Electronic mail: desimone@iom.cnr.it

^{f)} Electronic mail: grazioli@iom.cnr.it

^{g)} Electronic mail: raa@st-andrews.ac.uk

^{h)} Electronic mail: loelia.prt@gmail.com

ⁱ⁾ Electronic mail: iljp@st-andrews.ac.uk

ABSTRACT

A synchrotron based vacuum ultraviolet absorption spectrum for γ -pyrone has been interpreted in terms of singlet excited electronic states using a variety of coupled cluster, configuration interaction, and density functional calculations. The extremely weak spectral onset at 3.557 eV shows eight vibrational peaks, which following previous analyses, are attributed to a forbidden 1A_2 state. A contrasting broad peak with a maximum at 5.381 eV has a relatively high cross-section of 30 Mb; this arises from three overlapping states, where a 1A_1 state dominates over progressively weaker 1B_2 and 1B_1 states. After fitting the second band to a polynomial Gaussian function and plotting the regular residuals over 20 vibrational peaks, we have had limited success in analyzing this fine structure. However, the small separation between these three states clearly shows that their vibrational satellites must overlap. Singlet valence and Rydberg state vibrational profiles were determined by configuration interaction using the CAM-B3LYP density functional. Vibrational analysis using both the Franck–Condon and Herzberg–Teller procedures showed that both procedures contributed to the profiles. Theoretical Rydberg states were evaluated by a highly focused CI procedure. The superposition of the lowest photoelectron spectral band on the vacuum ultraviolet spectrum near 6.4 eV shows that the 3s and 3p Rydberg states based on the 2B_2 ionic state are present; those based on the other low-lying ionic state (X^2B_1) are destroyed by broadening; this is a dramatic extension of the broadening previously witnessed in our studies of halogenobenzenes.

© 2024 Author(s). All article content, except where otherwise noted, is licensed under a Creative Commons Attribution (CC BY) license (<http://creativecommons.org/licenses/by/4.0/>). <https://doi.org/10.1063/5.0186919>

I. INTRODUCTION

Recently, we reported a synchrotron-based redetermination of the photoionization spectrum for γ -pyrone,¹ a substance systematically described as 4H-pyran-4-one. The fully conjugated ring system depicted in Fig. 1 as structure 1a has raised the issue of whether the system is aromatic and also whether it supports a ring current.² Several studies by nuclear magnetic resonance (NMR)²⁻⁷ and microwave spectroscopy (MW)⁸⁻¹² have been performed in order to address these subjects and were discussed in Ref. 1. The detailed structure derived from the MW studies shows that the observed bond lengths support the classical formulation as in 1a, while the reactivity and substantial dipole moment, $3.79 \pm 0.02D$,¹⁰ point to the contributions of structure 1b. Furthermore, the $C_2=C_3$ double bond measured by MW spectroscopy is 1.344 \AA , almost the same as that for ethylene (1.339 \AA), while the C_3-C_4 single bond at 1.463 \AA is very close to cyclopentadiene (1.469 \AA); the $C_4=O_4$ double bond at 1.226 \AA is also very similar to that for acetone (1.222 \AA).¹⁰

The vibrationally averaged nematic phase γ -pyrone structures determined from 1H and ^{13}C NMR spectroscopy are also in close agreement with the MW results.¹³⁻¹⁵ Magnetic susceptibility anisotropies, analyzed by MW spectroscopy in terms of local and non-local contributions, show that both γ -pyrone and the related lactone (α -pyrone) have negligibly small non-local contributions; therefore, both are considered to be non-aromatic by this magnetic criterion. Theoretical results, near Hartree-Fock in quality for magnetic susceptibilities, and comparison with experimental values also seem to indicate that the 2- and 4-pyrones are non-aromatic.¹⁶ Fully optimized *ab initio* calculations on 4H-pyran-4-one (1a) and its three sulfur analogs, where one or both O-atoms are exchanged by S-atoms, and determination of the electrostatic potentials in four planes around the molecule lead to the conclusion that all four molecules are essentially non-aromatic.¹⁷

We now report a synchrotron-based study of the UV + VUV (vacuum ultraviolet) absorption spectrum for γ -pyrone in the energy range $3.344\text{--}10.78 \text{ eV}$, following our recent studies of azulene and other fully conjugated molecules.^{18,19} In the current study, we will use energy units of electron volts (eV) and wave number (cm^{-1}) but will refer to other units when used by other authors. There is a considerable body of information concerning the UV absorption of γ -pyrone.²⁰⁻²² This band lies close to the long-wavelength limit of our synchrotron spectrum, shown in black in Fig. 2. We have obtained the UV spectrum with a standard laboratory instrument, superimposed in blue. These two procedures provide an independent measurement for that energy region.

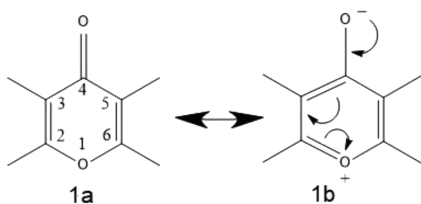


FIG. 1. Representations of the structure of γ -pyrone are shown in 1a and 1b; the high dipole moment is expressed by 1b, whereas the bond lengths as measured by microwave spectroscopy are close to those of the classical representation 1a.

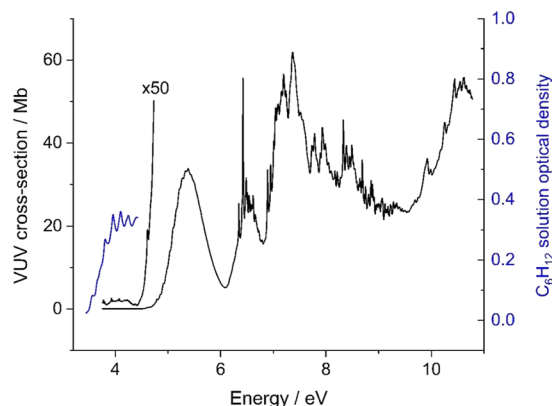


FIG. 2. The wide scan from the synchrotron absorption in the vapor phase, combined with the ultraviolet spectral results (shown in blue), for γ -pyrone in cyclohexane solution.

The UV absorption, conventionally denoted as the $S_1(\pi\pi^*)$ transition, was originally assigned to the forbidden $^1A_2 \pi\pi^*$ state as a set of eight maxima with λ_{max} 248 nm and electronic origin close to 3.516 eV .²² This S_1 band, spin-allowed but orbitally forbidden,²³ was thought to gain oscillator strength through vibronic mixing with $S_2(\pi\pi^*)$ or higher singlet $\pi\pi^*$ excited states.

CRD spectroscopy of phosphorescence by the lowest lying $\pi\pi^*$ T_1 state has led to a detailed analysis²⁴ of the 0^0 band origin as 3.384 eV . However, a supersonic free-jet expansion, where jet cooling eliminated congestion, led to a revised analysis.²⁵ An important conclusion was that time-dependent density functional theory (TDDFT) using the PBE0 functional gave more realistic vibration frequencies than the more computationally demanding equation of motion with coupled cluster singles doubles (EOM-EE-CCSD) method.²⁵ We will use the TDDFT method together with the CAM-B3LYP functional in the present study, as described in Sec. II.

Under the influence of UV light and at high concentrations, 4H-pyran-4-ones with phenyl substituents at C_3 and C_5 undergo dimerization to “head-to-tail” dimers, which are 2H-pyran-2-ones;²⁶ conversely, high dilution inhibits dimerization. The formation of pyran-2-ones from 4-ones with C_{2V} ring skeletons requires an unsymmetrical intermediate state; therefore, non-planar structures were also considered for singlet excited states of γ -pyrone.²⁶ This was abandoned when it became clear that the bulky C_3 or C_5 substituents must be responsible for the necessary twisting of the ring structure to occur.

II. METHODS

Following our previous study,¹ the γ -pyrone sample, CAS registry number 108-97-4, was synthesized by standard methods,^{27,28} and the purity was checked by 1H and ^{13}C nuclear magnetic resonance before use.

A. The spectral study

This was performed on different instruments for different energy regions.

1. Measurements in solution

The UV spectrum of γ -pyrone in the region of 280–360 nm (4.428–3.444 eV) was measured on a Shimadzu UV1600 instrument using a 10 cm path length cell at a concentration of 2.08 g/l in cyclohexane; the 402 data points were separated by 0.2 nm. Insufficient vapor pressure precluded the acquisition of the gas phase spectrum above 290 nm. The resulting spectrum is shown in blue in Fig. 2.

2. Gas phase measurements

The VUV–UV spectrum of γ -pyrone, shown in Fig. 2, was measured at 30 °C in the range 115–330 nm (10.78–3.757 eV) using the AU-UV beamline on the ASTRID2 synchrotron light source at the Department of Physics and Astronomy, Aarhus University, Denmark.²⁹ The setup used to measure this spectrum of γ -pyrone has been described in detail in a previous publication,²⁹ so only a brief summary will be given here. The AU-UV beamline, which takes light from a dipole magnet in ASTRID2, provides monochromatic light with a resolution of 0.08 nm using a 2000 lines/mm toroidal grating and 100- μ m entrance and exit slits. A gas cell enclosed with MgF₂ windows on the entrance and exit is mounted on the exit port of the beamline and evacuated using a turbo pump. The intensity of light passing through the cell over a range of wavelengths is measured using a photomultiplier tube on the exit of the cell, with and without the sample gas. The pressure in the cell is monitored using a heated 1 Torr capacitance manometer, with pressures chosen to ensure that attenuation of the incident light is low enough to avoid line saturation (typically 50% or less). Absolute photoabsorption cross-sections are then calculated using the known path length, $l = 15.5$ cm, of the cell using the Beer–Lambert law, $I_t = I_0 \exp(-N\sigma l)$, where I_0 is the incident light intensity, I_t is that transmitted with the gas in the cell, and N is the molecular number density determined from the pressure. Small sections of the spectrum are recorded with overlap, choosing the optimum pressure for the cross-section for each region to ensure that it is being measured without saturation effects. The beam current in the ASTRID2 light source, which runs in “top-up” mode, is continuously monitored, and the light intensity recorded by the photomultiplier is normalized to remove the effects of the decaying beam and injections.

B. Theoretical methods

Our study necessitates the use of several codes since no individual computational chemistry suite contains all the modules needed. The most inclusive is Gaussian Inc. version G-16,³⁰ which also contains the symmetry adapted cluster (SAC) configuration interaction code (CI),^{31–35} the vibrational analysis code originally from Pisa,^{36–38} and the time-dependent density functional theory (TDDFT) code.^{39–41} The principal functional used in this study was a long-range-corrected version of the Becke 3-parameter hybrid functional (B3LYP),⁴² described as the Coulomb-attenuating method (CAM-B3LYP).⁴³ Excited state adiabatic excitation energy (AEE) determination was carried out within TDDFT; this enabled equilibrium structures and harmonic frequencies for both valence and Rydberg states to be determined, and Franck–Condon (FC) and Herzberg–Teller (HT) vibrational analyses to be performed on the resulting wave functions. Vertical excitation energies (VEEs) were also determined by the use of the MRD-CI method⁴⁴ in

GAMESS-UK;⁴⁵ a description of this method is included in the supplementary material as SM1.

C. The principal basis sets

Atomic basis sets developed in recent years attempt to cover all types of excited states, with universal bases containing extremely high Gaussian exponents for states close to the nuclei and diffuse (exceptionally low exponents) for Rydberg states. We find it appropriate to treat these two types of states separately, as in our recent studies.^{19,46} We used triple-zeta valence with single polarization in all cases; this included using the 6-311G (d, p) basis set⁴⁷ in conjunction with the SAC-CI module^{31–35} of GAUSSIAN (G-16) and TZVP⁴⁸ with MRD-CI⁴⁴ of GAMESS-UK.⁴⁵ TDDFT is a single-configuration process; the excited state structure, determined theoretically, is used for both the ground and excited states. The potential energy surface in spectroscopy relies on differences between the potential energies of both upper and lower states at their equilibrium structures; we have introduced this correction when the vibrational states and their intensities are determined by the Pisa software. The results were subsequently enhanced by using the MRD-CI method.

III. RESULTS AND DISCUSSION

The X¹A₁ electronic state of γ -pyrone has C_{2v} symmetry^{8–10} with 25 doubly occupied molecular orbitals (DOMOs); 7 of these represent the core O_{1s}² and C_{1s}² electrons (5a₁² + 2b₂²). Throughout this study, we will use valence shell labeling for the doubly occupied molecular orbitals (DOMOs), which are 1a₁ to 8a₁, 1b₁ to 3b₁, 1b₂ to 6b₂, and 1a₂.

A. The theoretical γ -pyrone UV + VUV absorption spectrum

The theoretical manifold contains both valence and Rydberg states; the profiles for these states are shown separately in

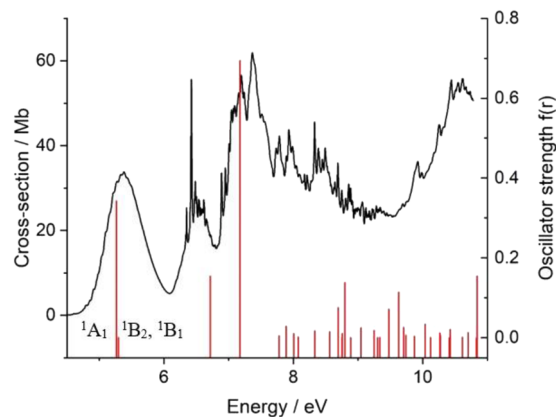


FIG. 3. The valence state vertical excitation energies for the singlet states, using the MRD-CI method and the TZVP basis set. The calculated energies, shown in red, are unscaled. There are three nearly degenerate states under the envelope between 5 and 6 eV; these are ¹A₁ (strong) < ¹B₂ < ¹B₁, which are both weak. A sharp vibrational structure is apparent in the peak close to 6.5 eV and must be attributed to Rydberg states, as described below.

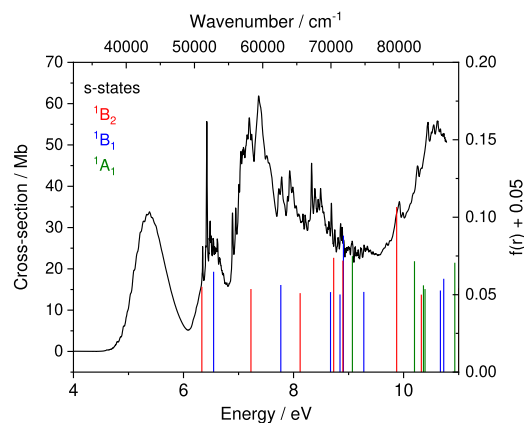


FIG. 4. The s-Rydberg states for 1B_1 , 1B_2 , and 1A_1 symmetries are shown in blue, red, and green, respectively. The oscillator strengths have been increased by 0.05 units to make them more distinct. The states shown are from calculations where both valence and Rydberg functions are present and, therefore, allow interactions between these two types of excited states.

Figs. 3 and 4, respectively. This is complex, owing to a wide intensity range with some broad bands and a sharp structure with close similarity to that of the photoelectron spectrum.¹ Semi-empirical calculations⁴⁸ of the lower singlet states for γ -pyrone suggest that the $n\pi^*$ state is lower in energy than $\pi\pi^*$ by $\sim 2000\text{ cm}^{-1}$ (0.248 eV).⁴⁸ Our study, shown in Table I, clearly shows the onset of the spectrum has four states, namely ${}^1A_2 \ll {}^1B_2 < {}^1B_1 < {}^1A_1$; these have widely different intensities, which are zero, medium, low, and very intense. We accept the proposition²⁴ that the forbidden 1A_2 state gains intensity by borrowing from the overlapping group of three states.

A principal objective of this study is to interpret the observed bands in the UV + VUV absorption spectrum over a wide range of vertical excitation energies (VEEs); these are shown in Table I. The valence states will form the basis of the most intense absorption, while the fine structure previously analyzed in the photoelectron spectrum will be present in the corresponding Rydberg states in absorption. We discuss these two types of absorption separately but first consider the effect of a change in theoretical method on the excitation energies observed; this enables common features to be identified.

B. Change in vertical excitation energies (VEE) with theoretical method

The SAC-CI study, our most rigorous procedure, was performed at the equilibrium structure of the X^1A_1 state for γ -pyrone, leading to predictions for the VEE of the excited states. The TDDFT method using the CAM-B3LYP functional generated the equilibrium structure for all the low-lying states. Since G-16 determines the adiabatic excitation energy (AEE) for both ground and excited states at the excited state structure, rather than in the spectroscopic method, where ground and excited state structures are independently determined at their equilibrium structures, we make a correction to the computed AEE to conform to the spectroscopic definition.

TABLE I. The valence states of γ -pyrone determined by the MRD-CI method together with the TZVP basis set. The lowest excited state, but not optically allowed, is 1A_2 at 3.952 eV. Where more than one term is shown, the density decreases from left to right both in this and related tables. For example, the lowest allowed (1A_1) state has densities of 0.894 and -0.263 ; it is coupled to the second 1B_2 state, which also has two leading terms, with densities of 0.921 and -0.173 .

Energy/eV	Oscillator strength	Symmetry	Leading terms
3.952	0.0	A_2	$3b_16b_2^*$
5.243	0.346	A_1	$3b_14b_1^* - 1a_22a_2^*$
5.266	0.014	B_2	$3b_12a_2^*$
5.298	0.000	B_1	$6b_22a_2^*$
6.716	0.154	B_2	$1a_24b_1^* - 3b_12a_2^*$
7.063	0.646	A_1	$1a_22a_2^* + 3b_14b_1^*$
7.640	0.017	A_1	$6b_27b_2^*$
7.780	0.005	B_2	$6b_29a_1^*$
7.790	0.011	A_1	$2b_14b_1^* + 3b_1^04b_1^{*2}$
7.840	0.028	B_1	$3b_19a_1^*$
8.054	0.002	B_1	$8a_14b_1^*$
8.149	0.014	A_1	$3b_15b_1^* - 2b_14b_1^*$
8.692	0.075	B_2	$6b_210a_1^* + 6b_212a_1^*$
8.710	0.002	B_1	$5b_22a_2 - 7a_14b_1^*$
8.737	0.001	B_1	$3b_111a_1^* + 3b_110a_1^*$
8.753	0.010	B_2	$6b_211a_1^* - 6b_212a_1^*$
8.798	0.138	B_2	$2b_12a_2^*$
9.219	0.018	B_1	$3b_110a_1^* - 3b_111a_1^*$
9.339	0.000	B_2	$1a_25b_1^* + 3b_13a_2^*$
9.474	0.071	B_2	$1a_26b_1^* + 1a_25b_1^* - 3b_13a_2^*$
9.591	0.022	A_1	$6b_28b_2^* + 2b_15b_1^*$
9.657	0.131	A_1	$6b_29b_2^*$
9.694	0.018	B_1	$1a_27b_2^* + 5b_22a_2^*$
9.862	0.007	B_1	$7a_14b_1^*$
10.115	0.020	B_1	$3b_112a_1^*$
10.124	0.011	A_1	$8a_19a_1^*$
10.277	0.013	A_1	$3b_17b_1^*$
10.407	0.000	B_2	$3b_13a_2^* - 1a_26b_1^* - 1b_12a_2^*$
10.672	0.135	B_1	$3b_113a_1^*$
10.746	0.041	B_1	$3b_114a_1^*$

We find a very tight correlation between these SAC-CI state energies and those from the TDDFT method. On a like-for-like symmetry comparison, i.e., A_1 with A_1 , B_1 with B_1 , B_2 with B_2 , and A_2 with A_2 , we find the correlation for the combined set is $CAM = 0.890(13)^*SAC + 0.562(145)$, where CAM and SAC are abbreviations for the energies using the respective methods; standard errors are in parentheses. For the range of states up to 10.0 eV VEE, the mean difference is 0.360 eV, while the maximum difference is 0.705 eV. The correlation is shown in the supplementary material under SM2. Recently, we observed a very similar correlation between SAC-CI and CAM-B3LYP energies for singlet states of quadricyclane.⁴⁶ Since these two methods have a very different demand on computing resources, this enables us to concentrate on the CAM-B3LYP at equilibrium much more cheaply; further, the TDDFT wave functions are compatible with the Franck–Condon and Herzberg–Teller vibrational suites. In contrast, the SAC-CI suite

is limited to providing information about the energy and oscillator strength of states.

A correlation between MRD-CI and the SAC-CI energy results yielded $\text{MRD} = 0.972(38)^* \text{SAC} + 0.645(378)$, where MRD is the abbreviation used for the MRD-CI methods; standard errors are in parentheses. The scatter between the SAC-CI and MRD-CI results is slightly larger, but the saving in CPU time is even larger than with CAM-B3LYP. Overall, these equations show that there is a close excitation energy relationship between the methods, and the correlation with the experiment could be performed with each; in the following sections, we use the MRD-CI as an example.

C. The valence shell singlet states

The highest occupied orbitals contain both π and lone-pair σ -orbitals. All the excitations shown in Table I are from the five-highest occupied MOs, and most are excited into one of the five-lowest VMOs. The groups of highest occupied and lowest unoccupied MOs are shown in Fig. 5. The lowest configurations leading to excited states with high oscillator strength are $\pi\pi^*$ states. Some of those shown in Table I have more than one leading configuration, and the dominant configuration is the first mentioned. As noted earlier, there are grounds for accepting that the 1A_2 state, classically forbidden in absorption, mixes with adjacent allowed states. The next three lowest excited states lie within 0.1 eV in energy but have significant differences in intensities.

All three states will exhibit vibrational structure, so these vibrations will clearly overlap each other, leading to extensive mixing of states of different symmetry. We are unable to evaluate these mixed states, so our interpretation of the observed spectrum will be

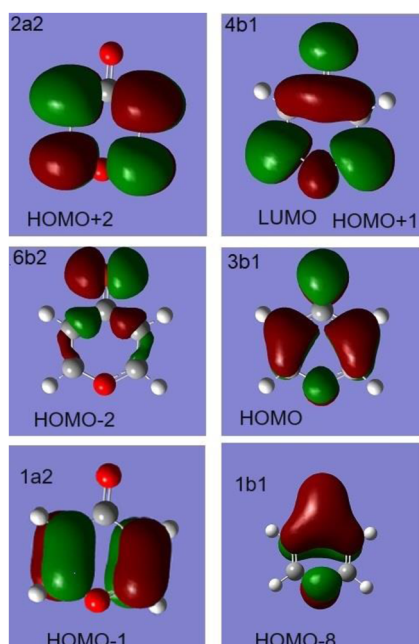


FIG. 5. Four of the highest occupied (HOMOs) and the two lowest unoccupied orbitals (LUMOs) for γ -pyrone. Many of the excitations shown in Table I feature these MOs.

limited. Although much vibrational structure has been identified, this must await further study. When we superimpose the classical profile, without mixing of states, on the experimental UV + VUV absorption spectrum, as in Fig. 3, only perturbed levels from the highest oscillator strength band will be apparent, with the second and third states either very weak or absent. Overall, most of the theoretical oscillator strength is limited to B_2 and A_1 symmetry states, and these must be correlated with the observed spectral intensity.

Several symmetric and antisymmetric combinations of $\pi\pi^*$ excitations occur; for the $3b_14b_1^* \pm 1a_22a_2^*$ pair of states, the separation is 1.82 eV, with the symmetric state lying at lower energy. These two states have the highest oscillator strengths of the calculated levels. Not only $\pi\pi^*$ states occur as linear combinations; the $\pi\sigma^*$ (1B_1) pair $3b_111a_1^* \pm 3b_110a_1^*$ is separated by 0.48 eV. Further details of these results are given in the supplementary material under SM3, which also contains a full set of roots, together with their oscillator strengths and second moments of the charge distribution (SECMOM). The latter gives a direct measure of the spatial volume of the natural orbitals. Valence states have values for the operators $\langle x^2 \rangle$, $\langle y^2 \rangle$, and $\langle z^2 \rangle$ close to those of the X^1A_1 ground state, which are -31.3 , -24.0 , and -36.8 a.u., respectively. These operators lead to markedly larger magnitudes for Rydberg states, some of which are shown below. Limited valence shell results using the coupled cluster method (SAC-CI) are shown in the supplementary material as SM4.

D. Vibrational analysis of the valence states

The complete assignment of the vibrational spectroscopy of the γ -pyrone ground state, including potential energy distributions (PED), has been studied in detail by Fausto *et al.*^{49a} Their experimental study also involved the isolation of the ground state in an argon matrix and Fourier-transform infrared spectroscopy.^{49b} Our comparison of the harmonic frequencies for the X^1A_1 state of γ -pyrone with its four lowest electronically excited valence states is shown in Table II. The present X^1A_1 results give a very close correlation with the Ar matrix data,^{49a} namely, $\nu_{\text{Calc}} = 1.063(7) - 34(12)$ with a correlation coefficient (adjacent R^2) of 0.9991; this includes the $\nu_{\text{C-H}}$ stretching vibrations, where the difference between theory and experimental $\nu_{\text{C-H}}$ averages 172 cm^{-1} . This correlation gives confidence that the values for the excited states in Table II are realistic. Furthermore, it enables us to adopt the nature of the vibrations from Fausto *et al.*'s PED analysis.^{49a} We note that they give an even closer correlation between their Hartree-Fock 6-31G* calculation and the Ar matrix values,^{49a} but all their frequencies were subjected to a single scaling factor of 0.89, whereas ours are unscaled.

Our relative energies and harmonic frequencies are shown in Table II. A single negative eigenvalue was obtained for both the 1B_2 and 1B_1 states; clearly, these are saddle points where small distortions to the symmetry must occur. We have been unable to complete a more sophisticated approach to get beyond this situation satisfactorily. The vibrational analyses were performed under both Franck-Condon (FC) and Herzberg-Teller (HT) selection rules for each of the lowest groups of valence states to check whether the HT was important to the analysis. C_{2v} symmetry was enforced, leading to the FC results for the lowest three states, 1A_1 , 1B_2 , and 1B_1 , as shown in Tables III-V.

However, when the FC + HT analyses were complete, it became apparent for the states shown in Table II that the FC intensity

TABLE II. Energies and harmonic frequencies for the X^1A_1 ground state and lowest valence excited valence states using the TDDFT methods.

Root	0	1	2	3	4
	X^1A_1	1A_2	1B_1	1B_2	1A_1
Energy/a.u.	-343.289 18	-343.143 03	-343.098 38	-343.092 56	-343.074 13
Oscillator strength	0	0.0	0.0000	0.0158	0.2043
	Frequencies/cm ⁻¹				
Mode and symmetry					
1 (A1)	3246	3265	3298	3284	3269
2	3225	3234	3270	3267	3225
3	1794	1689	1565	1542	1553
4	1716	1223	1477	1444	1441
5	1434	478	1383	1348	1318
6	1224	1441	1214	1177	1164
7	1031	1372	1061	1033	1004
8	953	1018	943	957	918
9	820	812	868	859	790
10	509	930	497	512	477
11 (A2)	1003	922	597	719	800
12	837	753	326	554	619
13	410	434	-251	112	297
14 (B1)	997	911	687	735	846
15	882	719	652	660	567
16	749	577	577	600	500
17	449	268	505	505	329
18	158	140	176	197	75
19 (B2)	3243	3259	3292	3269	3340
20	3225	3233	3288	3262	3225
21	1650	1591	2225	1419	2579
22	1446	1365	1428	1286	1379
23	1355	1271	1376	1228	1265
24	1238	1131	1282	1144	1051
25	1052	951	974	784	727
26	653	673	611	615	467
27	463	353	407	-232	329

results are dominant; some of the HT results are shown in the supplementary material. The full onset of the 1A_1 excited state shown in Table III includes all the principal types of excitation, whether weak or strong, but the intensities vary dramatically, both for the 0-0 bands and the vibrational satellites. Similar excitations occur in the full lists for the two other states in Tables IV and V, which are limited to the most prominent bands. As well as almost all the fundamentals (which are discussed below), their harmonics, which for some vibrations include up to eight quanta, binary, and multiple combination bands, are obtained. Since several bands having high intensity occur above 3000 cm⁻¹ relative to the 0-0 bands, one conclusion is that for closely spaced origins, as in Table II, the overlap of the vibrational states for the three states, 1A_1 , 1B_2 , and 1B_1 , will be inevitable.

The bands that are observed in the experimental spectrum then depend on both the intensities of the separate vibrational states and

any perturbations arising from interactions between them. The relative intensities of the separate states and the associated oscillator strength clearly indicate the visibility in the spectrum should be $^1A_1 > ^1B_2 \gg ^1B_1$, but unfortunately, the two weaker bands have lower 0-0 band energies, and the strong 1A_1 electronic state bands will occur under the tail of the vibrations from the less intense states.

Almost all of the single quanta of a_1 -fundamentals for the 1A_1 valence state in the Franck–Condon mode are observed. Mode 1 ($\nu_{C2-H} + \nu_{C6-H}$, labeled S_5) is included, while only mode 2 ($\nu_{C3-H} + \nu_{C5-H}$ S_4) is not listed, the a_1 vibration at 3225 cm⁻¹ following Fausto *et al.*^{49a} These are symmetric ν_{C-H} stretchings. However, mode 2 occurs as an overtone and in combination with mode 1. The most intense modes are 3¹ (1553 cm⁻¹) and 7¹ (1004 cm⁻¹), and the triple combination band is 5¹4¹1² (947 cm⁻¹). In the HT profile, all fundamentals are prominent but are ~1% of the intensity of the FC fundamentals.

TABLE III. The full onset of the Franck–Condon vibrational analysis of the 1A_1 valence state (fourth root) at the CAM-B3LYP level of valence states using the 6-311G(d,p) basis set; this includes both weak and strong bands, to demonstrate the wide variety of vibrational states, but includes all the fundamentals. Energy of the 0-0 transition: $46\,094\text{ cm}^{-1} = 5.715\text{ eV}$. All theoretical intensities are given as molar absorption coefficients ($\text{dm}^3\text{ mol}^{-1}\text{ cm}^{-1}$) in this study.

Energy/ cm^{-1}	Vibrational state	Intensity	Energy/ cm^{-1}	Vibrational state	Intensity
0	0	321 100	796	$5^1 4^1$	6470
151	1^2	29 250	809	$3^2 1^2$	1070
302	1^4	6096	809	$4^2 1^2$	4480
404	$3^1 1^1$	10 460	829	$7^1 3^1$	291
452	1^6	1382	857	$3^1 1^7$	407
477	10^1	18 800	881	$6^1 3^1 1^1$	814
555	$3^1 1^3$	4181	896	$8^1 3^1$	13 620
575	$7^1 1^1$	581	916	$9^1 2^1$	620
594	2^2	4816	918	8^1	27 990
603	1^8	322	933	5^2	815
628	$6^1 1^2$	2529	940	$11^1 1^2$	5168
643	$8^1 1^1$	2632	944	$8^1 1^5$	323
658	3^2	1073	947	$5^1 4^1 1^2$	321 100
659	4^2	34 590	959	$3^2 1^4$	29 250
706	$3^1 1^5$	1364	1004	7^1	127 900
726	$7^1 1^3$	244	1164	6^1	22 340
745	$2^2 1^2$	617	1318	5^1	5723
778	$6^1 1^4$	500	1441	4^1	21 320
790	9^1	37 890	1553	3^1	157 700
793	$8^1 1^3$	1020	3268	1^1	1193

Franck–Condon vibrational analysis of the 1B_2 valence state, shown in Table IV, is markedly weaker in intensity than that for the 1A_1 state, and we show only the stronger bands but include all fundamentals; the only vibrations absent are 2^1 (ν_{C-H}) and 8^1 (δ , in-plane bending).

The Franck–Condon profile for the 1B_1 state, shown in Table V, is remarkably weak but is reported with high precision in the hope that spectroscopically focused research on the 1B_1 state might extract these vibrations from the more intense states in this

region. Several fundamental modes are absent from the FC profile; indeed, some Herzberg–Teller fundamental vibrations are more intense than the Franck–Condon ones.

E. The calculated Rydberg state profile

After tests at various positions using the MRD-CI method,⁴⁶ the very diffuse Rydberg state functions (Gaussian functions, GTOs) were placed, together with the standard atomic basis functions, on

TABLE IV. Franck–Condon vibrational analysis of the 1B_2 valence state (third root) at the CAM-B3LYP level using the 6-311G(d,p) basis set; this concentrates on the fundamentals and intense binary vibrational states. The energy of the 0-0 transition is $41\,759\text{ cm}^{-1} = 5.177\text{ eV}$.

Energy/ cm^{-1}	Vibrational state	Intensity	Energy/ cm^{-1}	Vibrational state	Intensity
0	0	4251	2209.8767	$7^1 6^1$	1990
512.2493	10^1	1411	2354.1026	6^2	1503
859.2917	9^1	187	2476.9841	$7^1 4^1$	1527
1032.8254	7^1	2524	2574.4327	$7^1 3^1$	1967
1177.0513	6^1	3716	2621.2099	$6^1 4^1$	2142
1347.9301	5^1	391	2888.3173	4^2	1089
1444.1586	4^1	2834	3083.2145	3^2	2140
1541.6072	3^1	3702	3284.4489	1^1	39
1689.3006	$6^1 10^1$	1256	4116.0399	$7^1 3^2$	1110
2053.8566	$10^1 3^1$	1238	4260.2658	$6^1 3^2$	1641

TABLE V. Vibrational analysis of the 1B_1 valence state (third root) at the CAM-B3LYP level of valence states using the 6-311G(d,p) basis set. The energy of the 0-0 transition is $41\,188\text{ cm}^{-1} = 5.107\text{ eV}$.

Energy/cm $^{-1}$	Vibrational state	Intensity	Energy/cm $^{-1}$	Vibrational state	Intensity
0	0	2	1880.2595	5^110^1	0.426
497	10^1	1.126	1974.4500	4^110^1	0.344
1061	7^1	0.325	2061.6490	3^110^1	0.862
1214.3916	6^1	1.079	2428.7833	6^2	0.444
1303.0675	$15^2(b_1^2)$	0.008	2779.0634	3^16^1	1.237
1305.9575	$12^2(b_1^2)$	0.122	2947.9540	3^15^1	0.590
1383.2822	5^1	0.508	3042.1445	3^14^1	0.736
1477.4727	4^1	0.627	3129.3435	3^2	0.789
1564.6718	3^1	1.573	3276.0407	$3^16^110^1$	0.689
1711.3689	6^110^1	0.572	3297.6640	1^1	0.024

the carbonyl O-atom. The calculations were performed twice, once with only the valence state orbitals present and the second with the Rydberg functions added. The new MOs are Rydberg states within the valence set by comparison of eigenvalues and density matrix. There is a high density of states, as shown by visually combining the theoretical states in Figs. 3, 4, and 6. In the combined series, none of the eigenvalues are identical to those with only valence orbitals present. Therefore, each of the Rydberg states will inevitably be close to either a valence or Rydberg state enabling interactions. Similarly, the complex set of nuclei will provide an unevenly attractive force toward the Rydberg electron. All these factors will reduce the usual near-spherical symmetry of the electron distribution for the s-Rydberg states.

The energies of the calculated Rydberg 3s, 4s, and 5s states are shown in Table VI. All the extrapolated energies to the vertical ionization energy are low; the amounts are variable, but the four lowest

VIE lie between $\pm 0.5\text{ eV}$ of the experimental ones. When Cartesian functions are used for d- and f-functions, the $6d \rightarrow 5d$ and $10f \rightarrow 7f$ conversions to spherical harmonics are handled by the “harmonic” directive in GAMESS-UK⁴⁵ for the removal of the implicit s- and p-functions in 6d and 10f.

The principal s-Rydberg state energies are depicted in Fig. 4, where different colors are used for the B_1 , B_2 , and A_1 states. Similar diagrams can be drawn for the p-, d-, and f-states, as previously reported for quadricyclane.⁴⁶ It is clear from Fig. 4 that no Rydberg states lie under the spectral envelope below an excitation energy of 6 eV; therefore, the broadband close to 5.5 eV can only contain valence states. In contrast, the two Rydberg s-states shown in Fig. 4 with energies close to 6.4 eV must be the combined $3b_13s$ and $8b_23s$ Rydberg states, corresponding to the lowest ionization band reported for the PES previously.¹ The $3b_13s$ state, with a quantum defect $\delta = 0.864$, has a lower VEE of 0.207 eV (1668 cm^{-1}). The

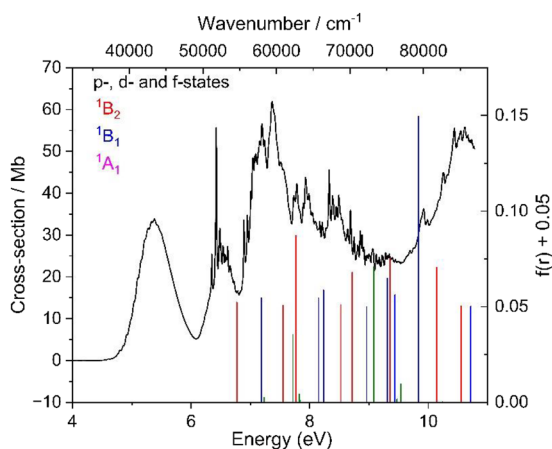


FIG. 6. The combined p-, d-, and f-Rydberg states as determined by a combined triple zeta and polarization basis set together with each of the Rydberg functions. Therefore, both valence and Rydberg functions are present in all these calculations, and the resultant roots contain both Rydberg states and low-lying valence states. One example of an intruder (valence) state lies near 9.8 eV. The calculated intensities have been increased by 0.05 units of oscillator strength to make the positions more obvious.

TABLE VI. The lowest calculated s-Rydberg states.

Energy/eV	Oscillator strength $f(r)$	Symmetry	State	Extrapolated VIE/eV
6.334	0.005	1B_2	3s	
7.226	0.004	1B_2	4s	8.639
8.119	0.001	1B_2	5s	
6.548	0.015	1B_1	3s	
7.768	0.006	1B_1	4s	9.410
8.844	0.000	1B_1	5s	
6.731	0.0	1A_2	3s	
7.757	0.0	1A_2	4s	10.848
8.435	0.0	1A_2	5s	
10.215	0.009	2^1B_1	3s	
11.327	0.002	2^1B_1	4s	12.647
12.007	0.000	2^1B_1	5s	
11.377	0.014	1A_1	3s	
12.222	0.012	1A_1	4s	13.710
13.232	0.004	1A_1	5s	

calculated separation of the two ionic states was 0.263 eV (2121 cm^{-1}).¹ The corresponding allowed 3p-Rydberg states, expected to lie close to 7 eV, are close to the onset of the most intense valence absorption and are discussed below.

F. The adiabatic excitation energies of γ -pyrone using the Rydberg basis

Extrapolation of the energies for each of the 3s, 4s, and 5s-Rydberg states to $n = \infty$ gives estimates of the vertical ionization energy with a single quantum defect (δ) by insertion in the equation: $VIE - E_n = 13.61/(n - \delta)$.² However, using such low quantum defects can make the extrapolated VIE unreliable. The Rydberg states, shown in Table VI, extrapolate to adiabatic ionization energies of 8.639 (303) with quantum defect 0.600(249) for 1B_2 and 9.410(34) eV for 1B_1 , with standard errors in parentheses. The corresponding extrapolated energies for the p -Rydberg states are 9.511 eV (1B_2) and 9.127 eV (1B_1), as are the ionization energies of the ionic states. Although not optically allowed, the 3s, 4s, and 5s-Rydberg states in 1A_2 symmetry can be projected to give an ionization energy value of 10.710 eV for the 2A_2 state, close to the observed value of 10.848 eV.¹ The corresponding set of 1A_1 s-Rydberg states by excitation from $8a_1$ leads to a projected ionization energy of 12.647 (163) eV, although lower than that assigned in the PES¹ at 13.25 eV, but the experimental onset is uncertain. The calculated sets of p -, d -, and f -Rydberg states, and any valence states intruding in the range, are shown in Fig. 4.

G. The experimental UV and VUV spectrum and its analysis

1. The energy range up to 4.5 eV

This shows an exponential rise from 3.5 to 4.5 eV with several local maxima, as seen in black in Fig. 7. The standard Boltzmann exponential function fit is shown in red, with further details of the fit in the supplementary material in SM6, while the regular residuals from this fit are in blue. The fit residuals allow a much sharper definition of the vibration frequencies, which were measured by

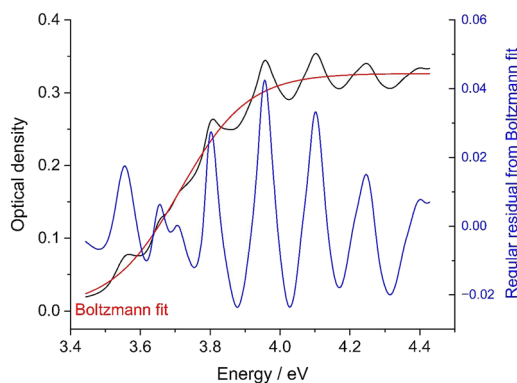


FIG. 7. The onset of the UV band, shown in black, has some poorly defined maxima. These are markedly sharpened by fitting to a Boltzmann function, as shown in red, and plotting its regular residuals, as shown in blue. The vibration frequencies from the 0-0 band, determined by electronic quadrature, are 813, 1218, 1989, 3222, 4405, 5561, and 6800 cm^{-1} .

mathematical fitting using the Origin Suite as mentioned in the supplementary material as SM7. The principal vibration frequencies are 813 and $1218 (\pm 20)\text{ cm}^{-1}$. This band is usually assigned to the forbidden 1A_2 state, which gains intensity by mixing with the complex band starting at 4.6 eV, as discussed below.

2. The energy range from 4.5 to 6.1 eV

This band is unusual since it is both wide in energy and complex in structure, with a series of undulations on the leading edge (low-energy side) up to the maximum and beyond. Fitting the spectral intensity data against a ninth-order polynomial of the energy removes the broad background and sharpens the undulations by using the regular residuals (in blue). These show, as in Fig. 8, that the undulations are significant since many occur as very sharp peaks. Our analysis of this spectral range is shown in Fig. 6. Assuming that γ -pyrone retains C_{2v} symmetry, the set of 4 low-lying states in Table I, calculated to lie in the energy range 3.9–5.3 eV (1A_2 , 1A_1 , 1B_2 , and 1B_1 in increasing energy order), creates a set of overlapping (mixed) states. Since the onset of the optically forbidden 1A_2 state is lowest in energy, its higher vibrational members will overlap directly with the pure 1A_1 and 1B_2 states; vibronic interaction is inevitable, with 1A_2 gaining intensity. The high intensity of 1A_1 relative to any bands in these other states may lead to the retention of some intensity in the now perturbed 1A_1 state. The wide range of their individual intensities in C_{2v} will lead to them all being perturbed together with the 1A_2 state, dominating in the linear combinations. We cannot offer a peak-by-peak analysis of the structure in Fig. 8. However, the sharp but weak peak, close to 4.6 eV, has the appearance of an 0-0 band followed by a vibrational manifold. Our interpretation, shown in Fig. 6, makes this 0-0 the origin of the perturbed 1B_2 lying on top of 1A_2 , the low intensity of the two states leading to little vibronic coupling. This is followed by an overlay with the strong 1A_1 state, which provides intensity for the main structure. We have measured the observed peaks, and these are listed in the supplementary material as SM(A). In our analysis, the 1B_1 state with near-zero intensity makes no contribution to the observed profile.

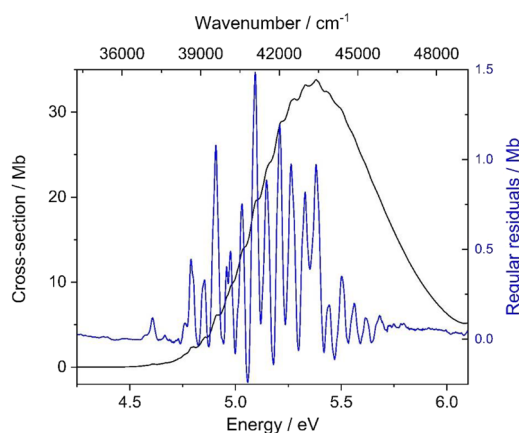


FIG. 8. The 4.5–6.0 eV region of absorption for γ -pyrone shown in black, with the regular residuals in blue after fitting to a polynomial in the energy, as discussed in the text.

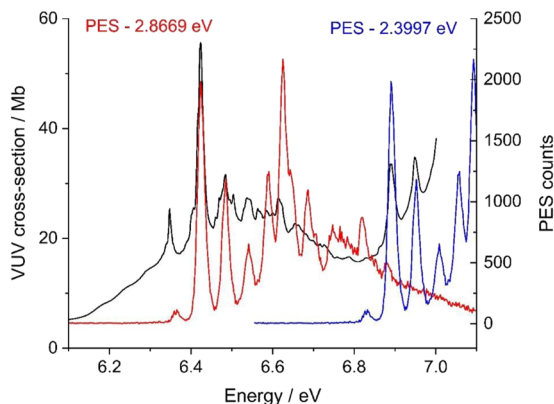


FIG. 9. The VUV energy range 6.1–7.1 eV, shown in black, with the photoelectron spectrum (PES) reduced by 2.8669 eV (in red) and 2.3997 eV (in blue) superimposed. Only in part of the PES does the lowest energy sequence of four peaks occur, which have portions of the VUV spectral profile. These correspond to the s and p Rydberg states, which have energies of 6.425 and 6.89 eV and quantum defects (δ) = 0.8212 and 0.6185, respectively, each with a principal quantum number $n = 3$.

3. The Rydberg state region between 6.1 and 7.1 eV in the VUV spectrum

The four lowest IEs of γ -pyrone (IE₁ to IE₄) show a well-defined vibrational structure with the energies (eV) shown in ²B₁ (9.291) as a composite band with ²B₂ (9.492), ²A₂ (10.840), and ²B₁ (12.650 eV). Using the 3s Rydberg states based on IE₁ of γ -pyrone and a predicted δ of 0.8, we have 6.479 (6b₂3s), 7.756 (3b₁3s); 9.104 (a₂3s), 10.914 (2b₁3s); these all lie in the energy range of the present VUV. Our recent PES analysis of the profile¹ clearly demonstrated that the complex band for γ -pyrone between 9.2 and 9.8 eV was for a two-state analysis; this gains further support from the Rydberg state analysis. This agrees with the theoretical profile for s-Rydberg states in Fig. 4, which also showed that none of these are predicted to lie below 6 eV. The onset of the band in the VUV spectrum at 6.348 eV corresponds to a weak peak in the PES.

The energy range where sharp (vibrational) structure first occurs is depicted in Fig. 9, where the photoelectron spectrum is superimposed twice in blue and red after lowering the energy of the PES lowest ionization band by 2.867 and 2.400 eV, respectively.

H. Assignment of the observed UV + VUV spectrum

The experimental onset of the γ -pyrone absorption, shown in Fig. 8, starts close to 4.6 eV and spreads to 6.1 eV, with a broad maximum close to 5.5 eV. The high intensity of 34 Mb is consistent with at least one allowed transition under the envelope. The lowest state is of ¹A₂ symmetry, at 3.852 eV, and is optically forbidden. The calculations in Table I then show a set of 3 nearly degenerate allowed states under the low energy part of the UV spectrum; the second root, a ¹A₁ state at 5.243 eV, has very high oscillator strength, but is followed by an almost degenerate ¹B₂ state at 5.266 eV and low $f(r)$, and then ¹B₁ at 5.298 eV, which has accidentally zero intensity.

This arises from the cancellation of finite contributions to the oscillator strengths from the leading configurations (3b₁9a₁* with 3b₁8a₁* and 3b₁7a₁*).

However, the principal cross-section under the envelope of the spectrum close to 5.4 eV must be the ¹A₁ singlet state dominated by the (3b₁4b₁* – 1a₂2a₂*) configurations. This onset peak clearly shows very weak undulations; these are resolved into a sharp set of peaks by removing a broad polynomial from the data points, with a maximum intensity of 1.48 Mb to be seen clearly, as in Fig. 8. Further details are shown in the supplementary material as SM1.

Theoretical interpretation of the regular residuals superimposed on the broad spectral band shown in Fig. 8 appears to require that a low intensity band occurs at the onset. The ¹A₁ state does not appear to be consistent with this since the calculated 0–0 transition, shown in Table III, has a high intensity for both Franck–Condon and Herzberg–Teller components; neither of these components or their combination will fit the observed vibrational sequence shown. We are forced to conclude that the degenerate ¹B₂ state lies lower in energy than the ¹A₁ state and that a two-state interpretation is present. The tail of the ¹B₂ then lies under the ¹A₁ state, leading to the loss of identity between both these and the even weaker ¹B₁ state. We believe that the origin of the ¹B₂ state is the 4.607 eV peak, which is a weak perturbation of the strong following ¹A₁ neighbor, which leaves some of the vibrations of the ¹A₁ state intact.

IV. CONCLUSIONS

Following our high-resolution photoelectron spectroscopy analysis of the spectrum of γ -pyrone,¹ we have presented the UV and VUV synchrotron-based absorption spectrum up to 10.78 eV (86 946 cm⁻¹) together with their analyses by density functional and configuration interaction. Both of these methods give close correlations to symmetry adapted coupled cluster methods. This is especially true of the CAM-B3LYP density functional in the TDDFT method when used with a triple-zeta basis, which includes polarization (TZVP, for example). We do not have software to perform vibrational analysis of the SAC-CI cluster wave functions, so the close correlation of these energies with TDDFT energies strengthens confidence that these latter results will reflect the higher-level calculated excitation energy variations.

The MRD-CI method is especially suitable for differentiating between Rydberg and valence states, and the prominent level of correlation capable of incorporation within it is a powerful asset.

The UV + VUV spectrum is deceptively simple at the low energy onset. A singular broadband, which is intense and 1.5 eV wide, is preceded by a very weak set of sharp peaks with extremely low intensity. We agree with a previous analysis²⁰ that assigned these sharp peaks to a perturbed ¹A₂ state, but we propose that it also includes a group of ¹A₁, ¹B₂, and ¹B₁ excited states with very strong, weak, and very weak intensities, respectively. Unfortunately, the two weak bands precede the very strong one; therefore, the latter will lie in the tail of the weak bands. Since the vibrational profiles of this group of three states will all overlay, it is inevitable that their vibrations will mix, and the very varied intensities will be perturbed.

In contrast, the 6.1–7.5 eV region contains a set of sharp peaks superimposed on broad, featureless valence states. Detailed analysis shows that these sharp states are the 3s and 3p Rydberg states leading to the lowest ionization energy, X²B₂. Comparison with

the photoelectron spectrum, where the overlap of the profiles of the X^2B_2 and A^2B_1 states had previously been proposed, confirms that situation. The A^2B_1 Rydberg states are absent, while the trailing vibrational structure from the X^2B_2 state is also perturbed. This situation is reminiscent of our earlier studies^{46,50–52} of the monohalogenobenzenes (C_6H_5X , where $X = F, Cl, Br, \text{ and } I$). In that series, we found that the overlap of the vibrational states from a lower lying ionic state led to progressive broadening of the higher energy vibrational states the closer the two systems were placed. Therefore, the normal peak width of an individual isolated peak on synchrotron-based PES can be neatly covered by a Franck–Condon peak with a half-width at half-maximum of 70 cm^{-1} , and one grossly widened peak may require 400 to 600 cm^{-1} to give a fit. Here in the UV–VUV, we have peaks effectively lost through broadening. The value of fitting undulating surfaces to polynomial functions to get the best fits, and then plotting the regular residuals from the fits, is a powerful route to disclosing new vibrational structure.

SUPPLEMENTARY MATERIAL

See the supplementary material for additional information on each of the following: (1) Details of the theoretical methods: (a) the MRD-CI method, (b) the SAC-CI method, and (c) Rydberg states. (2) The correlations between the symmetry adapted cluster configuration interaction, time-dependent density functional theory, and multi-reference multi-root methods. (3) Table SM3. The valence states of γ -pyrone determined by the MRD-CI method together with the TZVP basis set. (4) Table SM3. The valence states of γ -pyrone determined by the MRD-CI method together with the TZVP basis set. (5) Table SM5. Adiabatic excitation energies for γ -pyrone using the CAM-B3LYP functional in the TDDFT method for (a) valence states. (b) For Rydberg states where the basis set is extended to include s-Rydberg functions, this allows both types of states to be evaluated. (6) The onset of the UV spectrum is enhanced by the use of a Boltzmann function and plotting the regular residuals. (7) The electronically measured frequencies (cm^{-1}) from the 0-0 band at $28\,686\text{ cm}^{-1}$ (3.557 eV). (8) The TDDFT vertical excitation energies. (9) Tables III–V. Herzberg–Teller vibrational analysis of the valence states at the CAM-B3LYP level of valence states using the 6-311G(d,p) basis set.

ACKNOWLEDGMENTS

We acknowledge (a) ISA, Department of Physics and Astronomy, Aarhus University, for the beam time on the AU-UV beam line on ASTRID2; (b) The University of Edinburgh (Eddie3) and Edinburgh Parallel Computing Centre's (Cirrus) super-computing facilities for support; (c) numerical fitting was performed using Gnuplot-5.0.5;⁵³ (d) plotting used Origin 7.0;⁵⁴ (e) MOs were drawn by GaussView;⁵⁵ (f) AIM densities were evaluated using AIMQB; and T. A. Keith is acknowledged for the provision of this software.⁵⁶

AUTHOR DECLARATIONS

Conflict of Interest

The authors have no conflicts to disclose.

Author Contributions

Michael H. Palmer: Methodology (equal); Supervision (equal); Writing – original draft (equal). **Soren Vronning Hoffmann:** Data curation (equal); Investigation (equal); Methodology (equal); Project administration (equal); Supervision (equal); Validation (equal). **Nykola C. Jones:** Data curation (equal); Investigation (equal); Methodology (equal); Project administration (equal); Supervision (equal); Validation (equal). **Marcello Coreno:** Investigation (equal); Resources (equal). **Monica de Simone:** Funding acquisition (equal); Resources (equal); Supervision (equal). **Cesare Grazioli:** Data curation (equal); Investigation (equal); Supervision (equal). **R. Alan Aitken:** Conceptualization (equal); Methodology (equal); Resources (equal); Validation (equal). **Loëlia Perrault:** Methodology (equal). **Iain L. J. Patterson:** Methodology (equal).

DATA AVAILABILITY

The data that support the findings of this study are available within the article and its supplementary material and are available from the corresponding authors upon reasonable request.

REFERENCES

- 1 M. H. Palmer, M. Coreno, M. de Simone, C. Grazioli, N. C. Jones, S. V. Hoffmann, R. A. Aitken, and D. K. Sonecha, “The ionic and ground states of gamma-pyrone. The photoionization spectrum studied by synchrotron radiation and interpreted by configuration interaction and density functional calculations,” *J. Chem. Phys.* **158**, 014304 (2023).
- 2 H. C. Smitherman and L. N. Ferguson, “On the aromatic character of 4-pyrones,” *Tetrahedron* **24**, 923–932 (1968).
- 3 D. W. Mayo, P. J. Sapienza, R. C. Lord, and W. D. Phillips, “Exchange reactions of 4-pyrone and 4-pyrone derivatives,” *J. Org. Chem.* **29**, 2682–2685 (1964).
- 4 C. T. Mathis and J. H. Goldstein, “Proton magnetic resonance spectra of 4-pyrone, chromone and xanthone,” *Spectrochim. Acta* **20**, 871–878 (1964).
- 5 N. M. D. Brown and P. Bladon, “The proton magnetic resonance spectra of 4-pyrone, 1-thia-4-pyrone, 4-thiopyrone and 1-thia-4-thiopyrone,” *Spectrochim. Acta* **21**, 1277–1285 (1965).
- 6 R. E. Mayo and J. H. Goldstein, “Proton magnetic resonance and ^{13}C -H satellite spectra of 4-pyrone: Analysis and assignments,” *Spectrochim. Acta, Part A* **23**, 55–60 (1967).
- 7 V. Rutar and T. C. Wong, “Utilization of the improved resolution in two-dimensional polarization transfer NMR,” *J. Magn. Reson.* **53**, 495–499 (1983).
- 8 C. L. Norris, R. C. Benson, P. Beak, and W. H. Flygare, “Microwave spectrum of 2-pyrone and the molecular Zeeman effect in tropone, 2-pyrone, and 4-pyrone. Suppression of nonlocal contributions to the out-of-plane molecular magnetic bonyl group into an aromatic ring,” *J. Am. Chem. Soc.* **95**, 2766–2772 (1973).
- 9 R. C. Benson, C. L. Norris, W. H. Flygare, and P. Beak, “Classification of 2- and 4-pyrone as nonaromatic on the basis of molecular magnetic susceptibility anisotropies,” *J. Am. Chem. Soc.* **93**, 5591–5593 (1971).
- 10 J. N. MacDonald, S. A. Mackay, J. K. Tyler, A. P. Cox, and I. C. Ewart, “Microwave spectra, structures and dipole moments of 4H-pyran-4-one and its sulphur analogues,” *J. Chem. Soc., Faraday Trans. 2* **77**, 79–99 (1981).
- 11 G. Włodarczyk, J. Demaison, B. P. Van Eijck, M. Zhao, and J. E. Boggs, “Ab initio and experimental quartic centrifugal distortion constants of acetone, pyrazole, and γ -pyrone,” *J. Chem. Phys.* **94**, 6698–6707 (1991).
- 12 W. H. Flygare, “Magnetic interactions in molecules and an analysis of molecular electronic charge distribution from magnetic parameters,” *Chem. Rev.* **74**, 653–687 (1974).
- 13 J. W. Pavlik and L. T. Pauliukonis, “Photoisomerization of 4-pyrones. Nucleophilic trapping of reactive intermediates,” *Tetrahedron Lett.* **17**, 1939–1942 (1976).

- ¹⁴S. A. Spearman and J. H. Goldstein, "An NMR study of 4-pyrone oriented in two different lyotropic mesophases," *Spectrochim. Acta, Part A* **31**, 1565–1568 (1975).
- ¹⁵D. S. Williams and T. C. Wong, "The r_a structure of partially oriented 4-pyrone determined from ^1H NMR spectroscopy including the ^{13}C satellites," *J. Mol. Struct.* **101**, 297–303 (1983).
- ¹⁶A. Ligabue and P. Lazzaretto, "Theoretical determination of the magnetic properties of 2-pyrone and 4-pyrone, and *o*-benzoquinone and *p*-benzoquinone," *Mol. Phys.* **101**, 2497–2509 (2003).
- ¹⁷C. Thomson and C. Edge, "Ab initio calculations on 4H-pyran-4-one and its sulphur analogues," *J. Mol. Struct.: THEOCHEM* **121**, 173 (1985).
- ¹⁸M. H. Palmer, N. C. Jones, S. V. Hoffmann, R. A. Aitken, M. Coreno, M. de Simone, C. Grazioli, and I. L. J. Patterson, "The excited states of azulene: A study of the vibrational energy levels for the lower $\pi\pi^*$ -valence states by configuration interaction and density functional calculations, and theoretical studies of the Rydberg states," *J. Chem. Phys.* **157**, 154307 (2022).
- ¹⁹M. H. Palmer, S. V. Hoffmann, N. C. Jones, M. Coreno, M. de Simone, C. Grazioli, and R. A. Aitken, "The vacuum ultraviolet absorption spectrum of norbornadiene: Vibrational analysis of the singlet and triplet valence states of norbornadiene by configuration interaction and density functional calculations," *J. Chem. Phys.* **155**, 034308 (2021).
- ²⁰R. D. Gordon and W. K. C. Park, "The 353 nm $\pi\pi^*$ transition of 4H-pyran-4-one and a deuterated derivative," *Can. J. Chem.* **71**, 1672–1675 (1993).
- ²¹K. Yamada, "Infrared and ultraviolet spectra of α - and γ -pyrones," *Bull. Chem. Soc. Jpn.* **35**, 1323–1329 (1962).
- ²²N. Ishibe, H. Sugimoto, and J. B. Gollivan, "Electronic absorption and emission spectra of 4-pyrones, 4-thiopyrones and 4-pyridones," *J. Chem. Soc., Faraday Trans. 2* **71**(71), 1812–1822 (1975).
- ²³N. Ishibe, M. Sunami, and M. Odani, "Photoisomerization of 4H-pyran-4-ones to 2H-pyran-2-ones," *J. Am. Chem. Soc.* **95**, 463–468 (1973).
- ²⁴A. G. Sessions, M. P. McDonnell, D. A. Christianson, and S. Drucker, "Triplet and singlet (n,π^*) excited states of 4H-pyran-4-one characterized by cavity ringdown spectroscopy and quantum-chemical calculations," *J. Phys. Chem. A* **123**(29), 6269–6280 (2019).
- ²⁵L. M. Hoffelt, M. G. Springer, and S. Drucker, "Phosphorescence excitation spectrum of the $T_1(n,\pi^*) \leftarrow S$ transition of 4H-pyran-4-one," *J. Chem. Phys.* **128**, 104312 (2008).
- ²⁶S. W. Parsons, D. G. Hucek, P. Mishra, D. F. Plusquellic, T. S. Zwier, and S. Drucker, "Jet-cooled phosphorescence excitation spectrum of the $T_1(n,\pi^*) \leftarrow S_0$ transition of 4H-pyran-4-one," *J. Phys. Chem. A* **127**, 3636–3647 (2023).
- ²⁷E. R. Riegel and F. Zwilgmeyer, "Chelidonic acid," *Org. Synth.* **17**, 40–41 (1937).
- ²⁸C. De Souza, Y. Hajikarimian, and P. W. Sheldrake, "A convenient method for the preparation of pyran-4-one," *Synth. Commun.* **22**, 755–759 (1992).
- ²⁹M. H. Palmer, T. Ridley, S. V. Hoffmann, N. C. Jones, M. Coreno, M. De Simone, C. Grazioli, M. Biczysko, A. Baiardi, and P. Limao-Vieira, "Interpretation of the vacuum ultraviolet photoabsorption spectrum of iodobenzene by *ab initio* computations," *J. Chem. Phys.* **142**, 134302 (2015).
- ³⁰M. J. Frisch, G. W. Trucks, H. B. Schlegel, G. E. Scuseria, M. A. Robb, J. R. Cheeseman, G. Scalmani, V. Barone, G. A. Petersson, H. Nakatsuji, X. Li, M. Caricato, A. V. Marenich, J. Bloino, B. G. Janesko, R. Gomperts, B. Mennucci, H. P. Hratchian, J. V. Ortiz, A. F. Izmaylov, J. L. Sonnenberg, D. Williams-Young, F. Ding, F. Lipparini, F. Egidi, J. Goings, B. Peng, A. Petrone, T. Henderson, D. Ranasinghe, V. G. Zakrzewski, J. Gao, N. Rega, G. Zheng, W. Liang, M. Hada, M. Ehara, K. Toyota, R. Fukuda, J. Hasegawa, M. Ishida, T. Nakajima, Y. Honda, O. Kitao, H. Nakai, T. Vreven, K. Throssell, J. A. Montgomery, Jr., J. E. Peralta, F. Ogliaro, M. J. Bearpark, J. J. Heyd, E. N. Brothers, K. N. Kudin, V. N. Staroverov, T. A. Keith, R. Kobayashi, J. Normand, K. Raghavachari, A. P. Rendell, J. C. Burant, S. S. Iyengar, J. Tomasi, M. Cossi, J. M. Millam, M. Klene, C. Adamo, R. Cammi, J. W. Ochterski, R. L. Martin, K. Morokuma, O. Farkas, J. B. Foresman, and D. J. Fox, *Gaussian 16 Revision A.03*, Gaussian Inc., Wallingford CT, 2016.
- ³¹H. Nakatsuji and K. Hirao, "Cluster expansion of the wave function. Electron correlations in singlet and triplet excited states, ionized states, and electron attached states by SAC and SAC-CI theories," *Int. J. Quantum Chem.* **20**, 1301–1313 (1981).
- ³²H. Nakatsuji and T. Yonezawa, "Cluster expansion of the wavefunction. Satellite peaks of the inner-valence ionization of H_2O studied by the SAC and SAC CI theories," *Chem. Phys. Lett.* **87**, 426–431 (1982).
- ³³H. Nakatsuji, "Cluster expansion of the wavefunction, valence and Rydberg excitations, ionizations, and inner-valence ionizations of CO_2 and N_2O studied by the SAC and SAC CI theories," *Chem. Phys.* **75**, 425–441 (1983).
- ³⁴H. Nakatsuji, "Cluster expansion of the wave function. Ionization and excitation spectra of NO radical studied by the SAC and SAC-CI theory," *Int. J. Quantum Chem.* **24**(S17), 241–255 (1983).
- ³⁵H. Nakatsuji, K. Ohta, and T. Yonezawa, "Cluster expansion of the wave function. Spin and electron correlations in doublet radicals studied by the symmetry adapted cluster and symmetry adapted cluster-configuration interaction theories," *J. Phys. Chem.* **87**, 3068–3074 (1983).
- ³⁶V. Barone, J. Bloino, M. Biczysko, and F. Santoro, "Fully integrated approach to compute vibrationally resolved optical spectra: From small molecules to macrosystems," *J. Chem. Theory Comput.* **5**, 540–554 (2009).
- ³⁷J. Bloino, M. Biczysko, F. Santoro, and V. Barone, "General approach to compute vibrationally resolved one-photon electronic spectra," *J. Chem. Theory Comput.* **6**, 1256–1274 (2010).
- ³⁸A. Baiardi, J. Bloino, and V. Barone, "General time dependent approach to vibronic spectroscopy including Franck-Condon, Herzberg-Teller, and Duschinsky effects," *J. Chem. Theory Comput.* **9**, 4097–4115 (2013).
- ³⁹P. Hohenberg and W. Kohn, "Inhomogeneous electron gas," *Phys. Rev.* **136**, B864–B871 (1964).
- ⁴⁰W. Kohn and L. J. Sham, "Self-consistent equations including exchange and correlation effects," *Phys. Rev.* **140**, A1133–A1138 (1965).
- ⁴¹R. G. Parr and W. Yang, *Density-Functional Theory of Atoms and Molecules* (Oxford University Press, Oxford, 1989).
- ⁴²A. D. Becke, "Density-functional thermochemistry. III. The role of exact exchange," *J. Chem. Phys.* **98**, 5648–5652 (1993).
- ⁴³T. Yanai, D. P. Tew, and N. C. Handy, "A new hybrid exchange–correlation functional using the Coulomb-attenuating method (CAM-B3LYP)," *Chem. Phys. Lett.* **393**, 51–57 (2004).
- ⁴⁴R. J. Buenker and S. Krebs, "The configuration-driven approach for multireference configuration interaction calculations," in *Recent Advances in Multireference Methods, Recent Advances in Computational Chemistry* (World Scientific, 1999), Vol. 4, pp. 1–29.
- ⁴⁵M. F. Guest, I. J. Bush, H. J. J. Van Dam, P. Sherwood, J. M. H. Thomas, J. H. Van Lenthe, R. W. A. Havenith, and J. Kendrick, "The GAMESS-UK electronic structurepackage: Algorithms, developments and applications," *Mol. Phys.* **103**, 719–747 (2005).
- ⁴⁶M. H. Palmer, S. V. Hoffmann, N. C. Jones, M. Coreno, M. de Simone, C. Grazioli, R. A. Aitken, and C. Peureux, "High-level studies of the singlet states of quadricyclane, including analysis of a new experimental vacuum ultraviolet absorption spectrum by configuration interaction and density functional calculations," *J. Chem. Phys.* **158**, 234303 (2023).
- ⁴⁷M. J. Frisch, J. A. Pople, and J. S. Binkley, "Self-consistent molecular orbital methods 25. Supplementary functions for Gaussian basis sets," *J. Chem. Phys.* **80**, 3265–3269 (1984).
- ⁴⁸R. Ahlrichs and P. R. Taylor, "The choice of Gaussian basis sets for molecular electronic structure calculations," *J. Chim. Phys.* **78**, 315–324 (1981).
- ⁴⁹(a) R. Fausto, G. Quinteiro, and S. Breda, "Vibrational spectroscopy and *ab initio* MO study of the molecular structure and vibrational spectra of α - and γ -pyrones," *J. Mol. Struct.* **598**, 287–303 (2001); (b) J. Seixas de Melo, G. Quinteiro, J. Pina, S. Breda, and R. Fausto, "Spectroscopic characterization of α - and γ -pyrones and their substituted 4-hydroxy and 4-methoxy derivatives: An integrated infrared, photophysical and theoretical study," *J. Mol. Struct.* **565–566**, 59–67 (2001).
- ⁵⁰M. H. Palmer, T. Ridley, S. Vronning Hoffmann, N. C. Jones, M. Coreno, M. de Simone, C. Grazioli, T. Zhang, M. Biczysko, A. Baiardi, and K. A. Peterson,

“Combined theoretical and experimental study of the valence, Rydberg, and ionic states of chlorobenzene,” *J. Chem. Phys.* **144**, 124302 (2016).

⁵¹M. H. Palmer, T. Ridley, S. V. Hoffmann, N. C. Jones, M. Coreno, M. de Simone, C. Grazioli, T. Zhang, M. Biczysko, A. Baiardi, and K. Peterson, “Interpretation of the photoelectron, ultraviolet, and vacuum ultraviolet photoabsorption spectra of bromobenzene by ab initio configuration interaction and DFT computations,” *J. Chem. Phys.* **143**, 154303 (2015).

⁵²M. H. Palmer, T. Ridley, S. Vronning Hoffmann, N. C. Jones, M. Coreno, M. de Simone, C. Grazioli, T. Zhang, M. Biczysko, A. Baiardi, and K. A. Peterson,

“Combined theoretical and experimental study of the valence, Rydberg and ionic states of fluorobenzene,” *J. Chem. Phys.* **144**, 204305 (2016).

⁵³See [http://www.gnuplot.info/for Gnuplot Release 5.0.7](http://www.gnuplot.info/for%20Gnuplot%20Release%205.0.7) for more information about fitting procedures and error analyses.

⁵⁴*Origin Version 2019*, OriginLab Corporation, Northampton, MA, USA, 2019.

⁵⁵R. Dennington, T. A. Keith, and J. M. Millam, *GaussView, Version 6.1*, Semichem Inc., Shawnee Mission, KS, 2016.

⁵⁶T. A. Keith, *AIMQB (Version 14.11.23, Standard)*, T. K. Gristmill Software, Overland Park, KS, 2017, www.aim.tkgristmill.com.